CFD Simulation and Improvement of High-speed Twin Screw Compressors for Chillers

Bingqi Wang[1,*], Xiaokun Wu[2], Chuang Wang[1], Zhiping Zhang[2,3], Kai Ma[1], Ziwen Xing[1]

[1]Xi'an Jiaotong University, School of Energy and Power Engineering,
Xi'an, Shaan Xi, China
(starcraft@stu.xjtu.edu.cn)

[2]Gree Electric Appliances, INC.,
State Key Laboratory of Air-Conditioning Equipment and System Energy Conservation,
Zhuhai, Guang Dong, China
(wxiaokun@foxmail.com)

ABSTRACT

Twin screw compressors are widely adopted in chiller systems due to their high efficiency, reliability, and low maintenance. Increasing the speed of the compressor can reduce the manufacturing cost and the leakage. However, higher speed brings efficiency decay and noise increase. In our tests, increasing the speed of the original machine directly from 3000 rpm to 5000 rpm reduced the adiabatic efficiency by 7.5% with significant noise. To improve the performance of the twin-screw refrigeration compressor at a high speed of about 5000 rpm, 3D transient full-scale CFD simulations were performed with high-quality moving grids. The simulated results were validated by experiment results. The general non-reflection boundary condition (NRBC) and a damping method were adopted to speed up simulations. The pressure distribution inside the compressor chamber can be distinctly discovered and help guide the compressor design. The design parameters of the rotor, such as rotor configuration, wrap angle, and length ratio, were studied. With more lobes, the discharge pulsation can be reduced with slight performance improvement. The length ratio was optimized, and the relevance of the rotor tip velocity was discovered. Improvement can be made with a higher wrap angle at high speed, and the suction delay can also increase the efficiency at the same level. In addition, a parametric study of the design of the suction and discharge ports was carried out. It was found that a small depth of radial suction space can make the intake flow more directional and increase efficiency. Enlarging the suction port by using an unmatched wrap angle was also found to increase the efficiency. A parametric study of the discharge port with different built-in volume ratios was also performed, and a slightly enlarged port was found to be helpful for reducing the resistance. Utilizing the CFD method, additional improvement potential of screw compressors for chillers at higher speeds can be continually uncovered.

1. INTRODUCTION

In recent years, the problem of global warming and energy shortage has become increasingly prominent. The need for air conditioning in buildings accounts for over 20% of the world's total energy demand and is increasing. In these systems, the compressor, as the core component, accounts for most of the total consumed energy. Twin screw compressors are widely adopted in chiller systems due to their high efficiency, reliability, and low maintenance. The energy efficiency of screw compressors has a vital part to play in energy saving and reducing CO2 emission. A direct way to improve is by increasing the speed for lower leakage, which has been adopted in many air compressors. Besides, it is promising to save energy in systems with multiple compressors by replacing several at low speed with less at high speed. The operational speed of the air compressor can be over 16500 rpm (Kameya et al., 2011). However, the design speed of most twin compressors for chiller systems is only about 3000~4500 rpm. Although more speed can be reached, significant performance decay and noise can occur. Therefore, it is necessary to analyze and improve the performance of the twin-screw compressor at a high speed.

As speed and capacity increase, the uniformity assumption in the working chamber of screw compressors is not suitable, especially for compressors with low sound speed refrigerants like HFCs and HFOs. For example, in a compressor with R134a at 3000rpm, the pressure wave propagates about 7 mm per revolution of the male rotor, so it takes more than 30 degrees for the pressure to propagate from one side of a 250 mm length chamber to the other.

The pressure waves have been captured by sensors in Sun's (Sun et al., 2021, 2022) experiments. In Sun's tests, the measured indicator diagram is far from ideal compression, and the pressure even drops in compression. A dimensionless parameter for non-uniformity prediction was proposed in our previous study (Wang et al., 2023), and the chamber model is not recommended in non-uniform cases. With the development of the grid generation method (Kovacevic et al., 2014; Rane et al., 2013, 2021), transient analyses can be performed through computational fluid dynamics (CFD) using full-scale 3D numerical models. CFD can fully consider the 3D pressure distribution inside the working chamber, and the non-uniform distribution can also be captured. Further analysis and improvement at high speed can be performed using the CFD method.

The rotors decide the general geometry feature of screw compressors. The traditional 4+6 and 5+6 combination is most common, and more lobes configurations are becoming increasingly popular. As the number of lobes increases, the contact line length and the exhaust orifice area increase, while the area utilization factor and the blow hole area vary from large to small. With higher speed, the deficit of leakage through the contact line and blow hole can be reduced. Potential improvement can be achieved with more lobes by reducing discharge resistance and pulsation. Besides, the length diameter ratio at high speed still need to be investigated. Rotors with variable diameter and variable lead can also increase the suction and discharge port, which may improve performance at high speed. CFD simulation of variable lead has been performed (Rane et al., 2014), and several lead functions have been investigated. However, rotors with variable diameters and variable are not easy to manufacture. Increasing the wrap angle with constant lead can be a possible way. Utri (Utri & Brümmer, 2016) performed 1D simulations and compared rotors with different constant wrap angles and profiles. It was found that the efficiency increased with a 350° wrap angle compared to 300° due to lower flow resistance. Besides, fluids with a low speed of sound and a low isentropic exponent, such as HFCs and HFOs, were found to have more potential for large wrap angle or dual lead compressors (Utri & Brümmer, 2017).

The suction and discharge ports also influence the performance of the compressors. The built-in volume ratio, Vi, is determined by the shape of the discharge port. Enlarging the discharge port is a possible method to reduce flow resistance, especially for low-pressure-ratio applications. However, large discharge ports could also cause pressure pulsation and power loss. Modifications to the suction ports of chillers offer an alternative approach for reducing the flow resistance through the suction port of twin screw compressors. The suction delay angle has been studied by many researchers (Cambio et al., 2021; Kameya et al., 2011; Sun et al., 2022) and has been verified by experiment. A parametric study was performed in our previous study and indicated more delay is required with higher speed (Wang et al., 2024). However, the suction port can invade the contact line at high speed with a large delay angle, and the specific shape still needs to be investigated. The optimal suction arrangement can also be different with high rotor tip velocity. In experiments with air compressors, it has been found that additional radial suction ports reduce performance(Pascu et al., 2013). With more dense fluid and higher speed, the radial suction port could also decrease performance, and further investigation is required.

In summary, this study aims to improve the efficiency of twin-screw compressors for chillers at high speed, especially at 5000 rpm. The original machine was simulated and tested at high speed. Based on the results, the pressure distribution and power consumption were analyzed. After that, a parametric study of the design parameters of rotors and ports was performed. Finally, a new machine was designed and compared with the original one by simulation. In this paper, the basic guide is provided for designing screw compressors at high speed.

2. Methodology

Numerical analysis was carried out using the ANSYS CFX solver to study the performance of compressors with various configurations. The fluid domain and the CFD settings are listed in this section. The mesh-independent test was performed, and the non-reflection boundary was discussed here.

2.1 CFD Model

The rotor configuration of the original machine is 5+6, and the distance between the centers of the female and male rotor is 128 mm. The male rotor is 250 mm in length with a wrap angle of 300°. The theoretical volume flow rate is 566.4 m^3/h at 3000 rpm. The actual fluid domain consists of three parts: the motor, the rotor, and the discharge pipe, as shown in Figure 1 (a). However, the complexity of the geometry of the actual model leads to a large number of meshes and is time-consuming. Therefore, a simplified flow domain containing only the rotor part was also adopted here in the parametric study, as shown in Figure 1 (b).

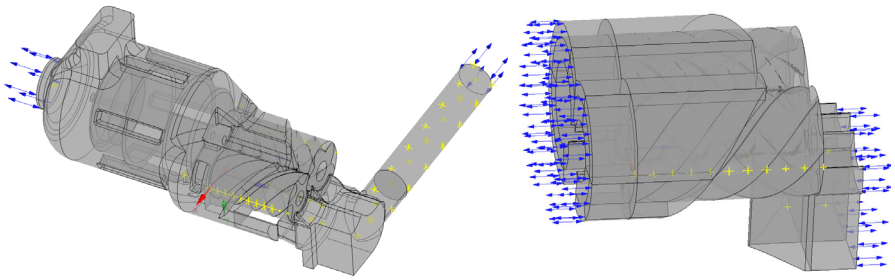

(a) Actual model (b) Simplified model

Figure 1: Fluid domain

The governing equations adopted in CFD simulations have been described in former research, and more details can be found in Rane's study(Rane et al., 2013, 2014). Second-order time and space discretization were adopted here. The time step was set as the male rotor rotated 1°. *k-ω* SST turbulence model was used here as the high Re flow in the compressor chamber as suggested by (Rane et al., 2014). The working fluid is R134a, and the ARK model was adopted here. The comparison of the real gas model can be found in (Rane et al., 2021). The rotor tip, interlobe, and end face clearances are all set at 0.03mm to simulate the sealing effect of the oil. Operating conditions are 5/36 °C, with a suction superheat of 5 °C. More details of the setting can be found in Table 1.

Table 1: Detailed settings of CFD simulation

Item	Value	Item	Value
Advection scheme	High resolution	Evaporation temperature	5°C
Transient scheme	Second-order backward Euler	Condension temperature	36°C
Thermal equation	Total energy with viscosity heat	Inlet pressure	349.66kPa
Time step	1°	Inlet temperature	10°C
RMS criterion	10^{-4}	Inlet turbulence intensity	5%
Turbulence model	*k-ω* SST	Outlet pressure	910.92kPa
Working fluid	R134a	Outlet temperature	45°C
Equation of state	Aungier Redlich Kwong	Outlet turbulence intensity	Zero gradient
Clearance	0.03 mm	Oil inlet temperature	40°C

2.2 Mesh Independent Test

The stationary part of the simplified fluid domain can be easily sliced and meshed by high-quality hexahedronal elements. The deforming part is complex due to the moving of rotors. The Twinmesh software developed by CFX Berlin was adopted here to generate high-quality dynamic grids. The circumference division of the female rotor is set as 360, as the 1° time step, and the mesh size of the male rotor is set as 1.8mm. However, there is no clear guide for the axial and radial divisions. Therefore, a mesh-independent test was performed in this paper, and the results are shown in Table 2. By comparing grids 1 and 2 and grids 7 and 8, it can be seen that the number of radial divisions slightly affects the simulated mass flow rate. Conversely, the number of axial divisions plays a vital role in the simulation. 40 or 100 divisions, as adopted in some previous studies, does not seem enough. From grids 5 to 7, the mass flow rate continually increases with the axial division number. Ideally, the number of axial divisions should be proportional to the wrap angle, not based on the mesh size. As the mesh is more sensitive to axial divisions than radial divisions, grid 7 is chosen finally.

2.3 Influence of Oil Injection

In the tested machine, minimum oil is injected to lubricate the contact region of the male and female rotors. In this paper, a small clearance of 0.03mm is adopted to simulate the sealing effect of the oil. Several simulations with the multiphase model were performed to validate this approach. The inhomogeneous model without the free surface option was applied, and an interface length scale of 5 microns was specified (Basha et al., 2018). The speed is 5000 rpm, and the maximum flow rate of the injected oil is 300 $kg \cdot h^{-1}$. Simulated results are shown in **Figure 2** (a). It can be seen that the mass flow rate is hardly affected by the injected oil, indicating that the small clearance is enough to simulate the sealing effect. Meanwhile, the change in shaft power is almost proportional to the injection flow rate,

and 300 kg·h^{-1} injection rate increased the shaft power by about 1.4%. As shown in **Figure 2** (b), the influence of oil on gas temperature is not obvious. In our tests, the oil injection port was closed, and only a small amount of oil entered the chamber through the bearing at a flow rate of less than 100 kg·h^{-1}. So, the following simulation shall be performed in a single phase, as the multiphase model is time-consuming and unstable.

Table 2: Mesh-independent test

No.	Radial division	Axial division	Mass flow rate/kg·s^{-1}	Deviation
1	5	40	2.0176	-17.74%
2	5	100	2.3635	-3.64%
3	10	40	2.0310	-17.19%
4	10	100	2.3715	-3.31%
5	16	120	2.4012	-2.10%
6	16	160	2.4281	-1.00%
7	16	200	2.4478	-0.20%
8	20	160	2.4336	-0.78%
9	20	200	2.4527	0.00%

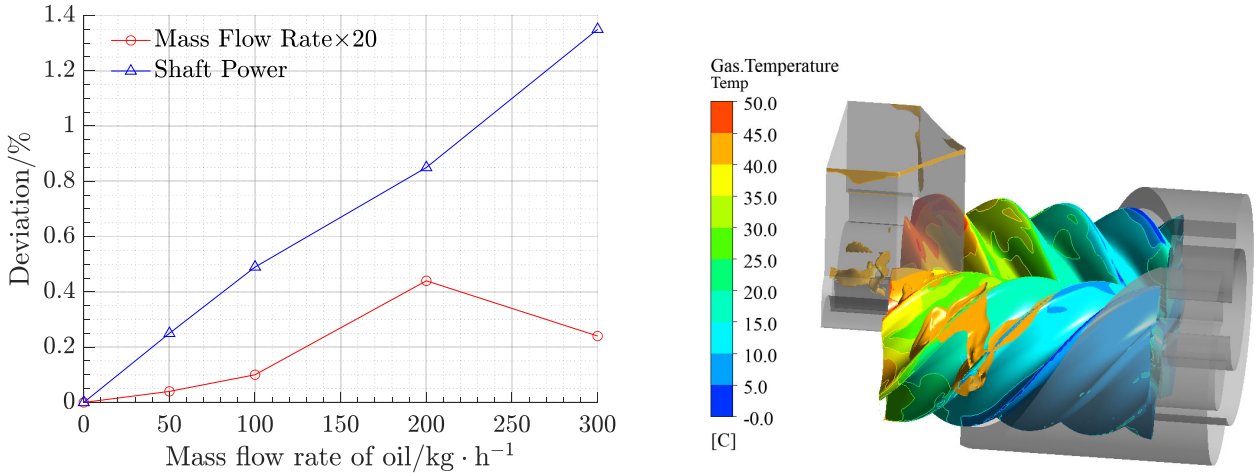

(a) Deviation by oil flow rate (b) Isosurface of 1% vol at 300 kg·h^{-1}

Figure 2: Influence of oil Injection

2.4 Non-reflection Boundary

In previous studies, the inlet and outlet boundaries were usually set as fixed pressure or total pressure. Normal pressure boundaries lead to numerical reflections and repetition of pressure waves in the computational domain. In order to make the pressure wave pass through boundaries, non-reflective boundary conditions (NRBC) are needed. The NRBC method has been widely adopted in the 1-D pipeline and 3-D acoustic FEM simulations. In the field of CFD simulation of compressors, Andres (Andres et al., 2022) also mentioned NRBC, but there is still no clear guidance on NRBC. In this paper, the simulation results with and without NRBC are compared using an actual fluid model, and the reflection length scale is set as

$$L_{ref} = \frac{c}{z_1 n / 60} \tag{1}$$

where, c is the sound speed, m·s^{-1}; z_1 is the lobe number of the male rotor; n is the rotational speed of the male rotor, rpm. The reflection relax factor is set as 0.15 and 0.35, and the results are shown in Figure 3. It can be seen in the average lines of the mass flow rate that it is hard to converge without the NRBC. The reason is that the reflection of the pressure wave causes fluctuations in the outlet mass flow rate. As the rotational speed increases, the length of each time step decreases, and the distance over which the pressure wave travels within each step is smaller, which results in a pressure wave that is more difficult to dissipate. For complex geometries and high rotational speeds, even more than 10,000 time steps are required for convergence. At the same time, the average mass flow rate

converges into a stable value in 5000 time steps with the NRBC. This indicates that the NRBC is vital to speed up the simulation progress, especially at high speed. The eigenvalues in NRBC have adopted the ideal gas assumption, but it still works well. In addition, it should be noted that the outlet pressure is not a specified value with NRBC, and this is important for pulsation analysis. The average flow rate does not change with the relaxation factor but converges faster with a 0.15 factor, which is recommended.

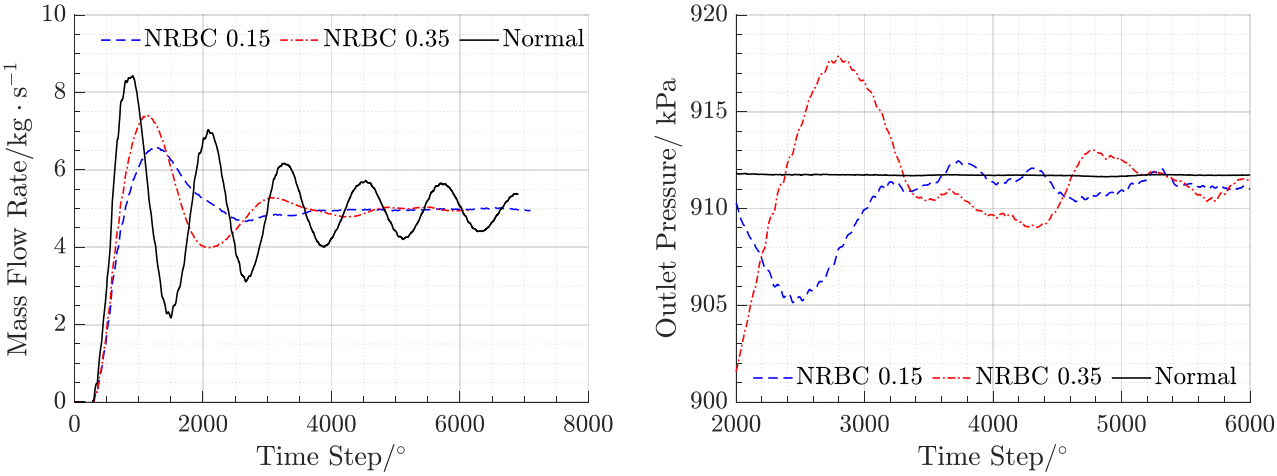

(a) Mass flow rate (360° Averaged) (b) Pressure (360° Averaged)

Figure 3: Simulation results at the outlet boundary with NRBC condition

However, the NRBC is unstable in simulation. In our tests, it cannot converge as the relax factor is 0.25. An alternative solution is the absorbing elements, but the pressure loss may influence the results and, therefore, need to be adjusted. In this paper, a time-dependent damping method is proposed by introducing an additional source term. The domain is regarded as porous and reduces the reflection at initial. Then, the domain is gradually converted into a normal domain by reducing the source term. The source term formula for the porous domain is

$$\boldsymbol{S}_{M,i} = -\frac{\mu}{K_{\text{perm}}} U_i - K_{\text{loss}} \frac{\rho}{2} |\boldsymbol{U}| U_i \tag{2}$$

where, S_M is the source term;i is the coordinate direction; μ is the dynamic viscosity; ρ is the density; $\boldsymbol{U}$ is the velocity vector; K is the coefficient. A more direct way is to define the linear resistance coefficient as

$$C_{R1} = \frac{\mu}{K_{\text{perm}}}, C_{R2} = K_{\text{loss}} \frac{\rho}{2} \tag{3}$$

The CR1 should gradually come to 0, and here, an S-type function is adopted as

$$C_{R1} = \frac{c_1}{\exp(\theta/360 - c_2)} \tag{4}$$

where, θ is the accumulated rotated angle, degree; c_1 is the damping strength factor, 1000-10000 is recommended; c_2 is the damping range factor, 2-10 is recommended. The simulation results are shown in Figure 4 with c_1=4000 and c_2=6. It can be seen that the average flow rate converges with the damping method as fast as the NRBC method. It can also be used in the suction domain and has good results, in which case the NRBC method failed to converge. However, this method is not suitable for studying the pulsation as the boundary reflection still exists. It can be seen that the fluctuation amplitude of the outlet flow rate with the damping method is more significant than that with the NRBC method. A possible solution is combining two methods, which need further study.

2.5 Experimental validation

An experimental test was performed and compared with the simulated results, as shown in **Figure 5**. The test rig is the same as that in our previous study(Wang et al., 2024). A linear additional power loss factor, including motor efficiency and mechanical friction loss, is multiplied by the simulated results, defined as -2.5×10^{-5}n + 0.965. The experimental results show that the adiabatic efficiency gradually decreases with increasing rotational speed. When the rotational speed is increased from 3000 rpm to 5000 rpm, the efficiency decays by about 7.5% and the CFD shows the same result. The simulated efficiency decreases by about 3.5% without considering the additional power

loss, mainly caused by flow resistance. In general, the CFD result can represent the general trend in the experiments.

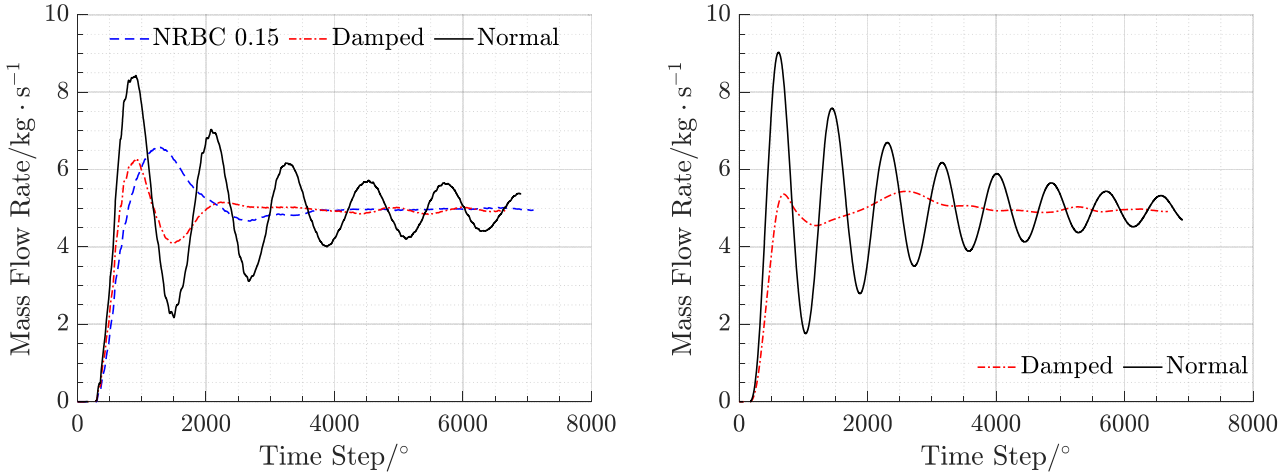

(a) Outlet (360° Averaged) (b) Inlet (360° Averaged)

Figure 4: Mass flow rate at boundaries with damping method

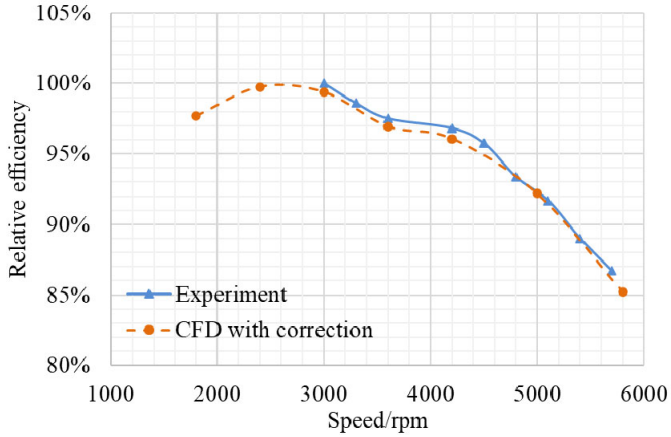

Figure 5: Simulated results compared with experimental results.

3. Results and Discussion

The target flow rate of the newly designed machine is 1291.3 $m^3 \cdot h^{-1}$ at 5000 rpm, which is a 36.9% increase in volumetric flow per revolution compared to the original machine. Several parametric studies are performed using the simplified fluid domain. The new machine is developed and simulated using the actual fluid domain.

3.1 Rotor Configuration and Length Ratio

In the test of the original machine, a huge noise occurs at high speed. A possible solution to reduce the pulsation and noise is increasing the number of lobes. However, the area of the blow hole will increase, and efficiency decay could occur. Therefore, different rotor configurations are simulated and compared. As the flow rate increased, the rotor with 5+6 configuration was 330 mm in length and 136 mm in center distance. Rotors with different configurations were generated at the same length and the theoretical volumetric flow rate. The comparison results are shown in Figure 6, where the isentropic efficiency changes are minor. The 7+8 configuration is chosen for higher efficiency and easier manufacturing than 8+9.

The length-diameter ratio, a vital rotor parameter, is also investigated. A large L/D ratio helps reduce the rotor tip velocity and increase the area of the radial discharge port. However, the contact line is also extended, which causes

more leakage. Conversely, a small L/D ratio results in high rotor tip velocity and more flow resistance. A parametric study was performed at 5000 rpm, and the results are shown in **Figure 7**. It can be seen that the optimum aspect ratio for 7+8 rotors is about 1.64, and for 5+6 rotors is about 1.1-1.6. The trend of efficiency with rotor tip speed is similar for different rotor configurations. The L/D ratio of 1.64 is selected, and the rotor length is 330mm. In addition, it is recommended that the rotor tip should not exceed 0.35 Ma.

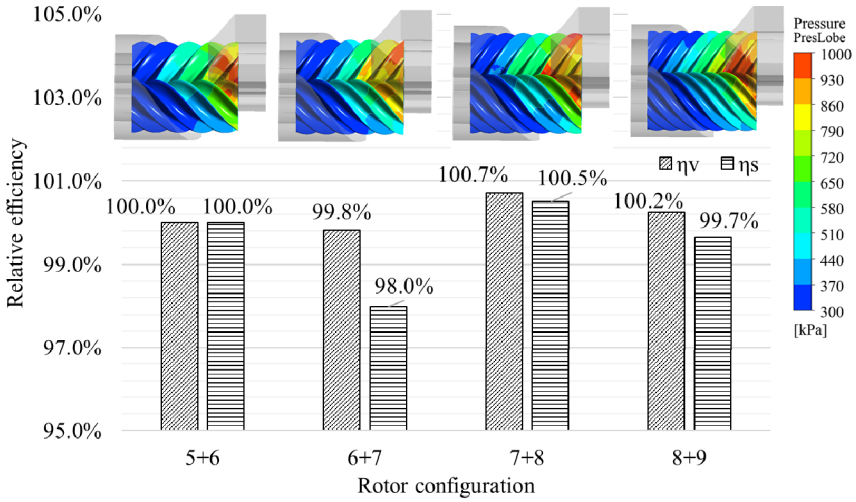

Figure 6: Relative efficiency with different rotor configurations

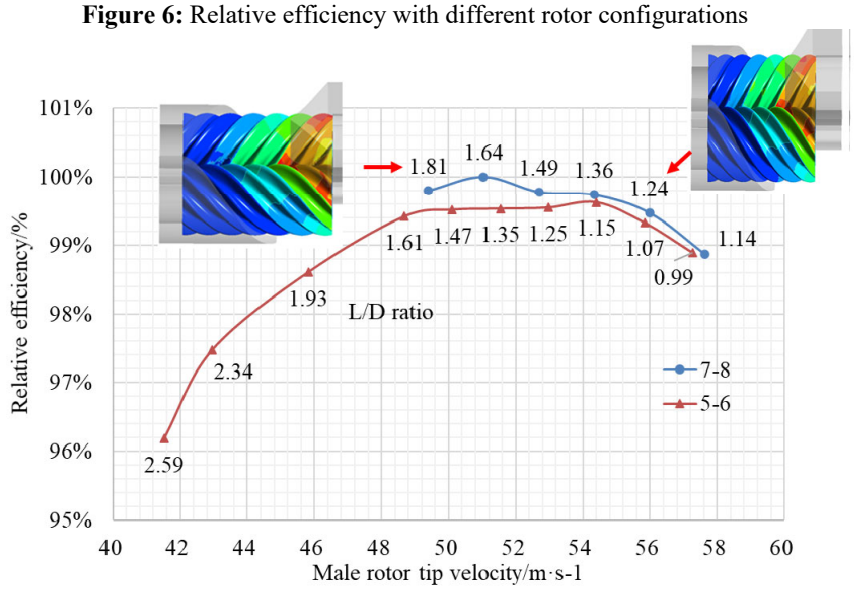

Figure 7: Relative efficiency with L/D ratio

3.2 Wrap Angle and Suction Delay

The wrap angle of the rotor is also essential for performance improvement at high speed, which has been experimentally verified in our previous study(Wang et al., 2024). With a higher wrap angle, the axial suction port and discharge port can be enlarged, and the flow resistance can be reduced. According to our previous study, wrap angles over 330° are selected and compared. The results are shown in Figure 8, where the efficiency increases as the wrap angle increases from 330° to 360°. As the wrap angle increases to 340°, the efficiency increases by about 1.25%, then the rate of increase slows to about 2.10% at 360°. However, the overlap constant decreases with the wrap angle, and the volumetric flow rate has a 2% decay at 360°.

In our previous study, the axial suction port was found to impact efficiency significantly at high speed, and a suction delay strategy was adopted. Therefore, the axial suction port is also investigated. Two improved axial suction ports at 330° were tested: 330Delay delays axial suction port disengagement by 16°, and 330Full opens the suction port completely. As shown in Figure 8, the efficiency of the two modified ports increases by about 2%. In addition, with a wrap angle of 360°, the axial suction port will invade the contact line. Two improved axial suction ports at 360° were tested: 360Cut removes the part of the axial suction port that intrudes into the area enclosed by the contact line, and 360Full opens the suction orifice port completely. However, the efficiency of these two modified ports has hardly increased.

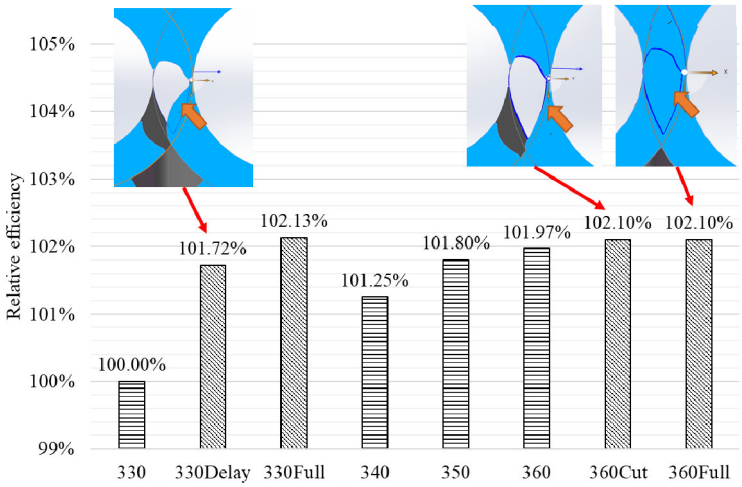

Figure 8: Relative efficiency with wrap angles

Further analysis can be performed by pressure distribution at the suction port, as shown in Figure 9. At the end of the suction process of case 330, there is a low-pressure region due to the flow resistance. If the suction end is delayed, as shown in case 330Delay, more fluid can be taken. In this case, the low-pressure region disappears, and the efficiency can be improved. Actually, the suction port of case 360 is close to 330Delay, which indicates that the flow resistance of the suction port may have more impact on efficiency than the discharge port. The efficiency can be further improved in the case of 330 Full, as the required delay is far more than 16° at 5000 rpm. In cases of 330Full and 360Full, the low-pressure region caused by the initial volume increase has vanished, which could help reduce the noise and vibration. 330 Full and 360 Full have similar efficiencies, but 330 Full has a 2% higher volume flow rate, so 330 Full is recommended.

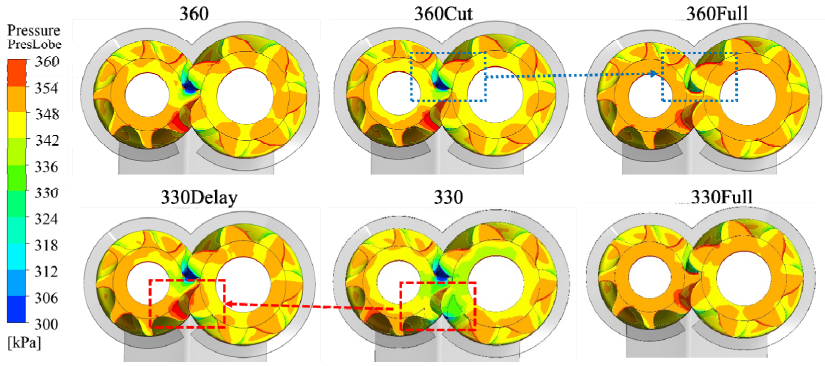

Figure 9: Pressure distribution at the suction port

3.3 Design Parameters of Ports

The design parameters of ports have also been investigated, and the parameter study was performed in the case of 330 Delay. The results with different radial suction ports are shown in Figure 10. By delaying the radial suction port, the efficiency can be slightly improved. The area of the radial suction port can be enlarged by decreasing the wrap angle of the port. An efficiency improvement is expected by decreasing the area of the radial suction port and

avoiding contact with the high-pressure area near the discharge side. However, the length of the radial suction port is set at 200mm, which is not fully extended, and the high-pressure area is excluded. In this case, an enlarged port with a smaller wrap angle reduces the resistance and improves the performance. In addition, reducing the depth of the radial suction port also contributes to efficiency, as a more oriented flow pattern facilitates the recovery of kinetic energy. A radial suction port with a 5-10 mm depth is recommended. Smaller depths increase the resistance to flow and lead to a decrease in efficiency.

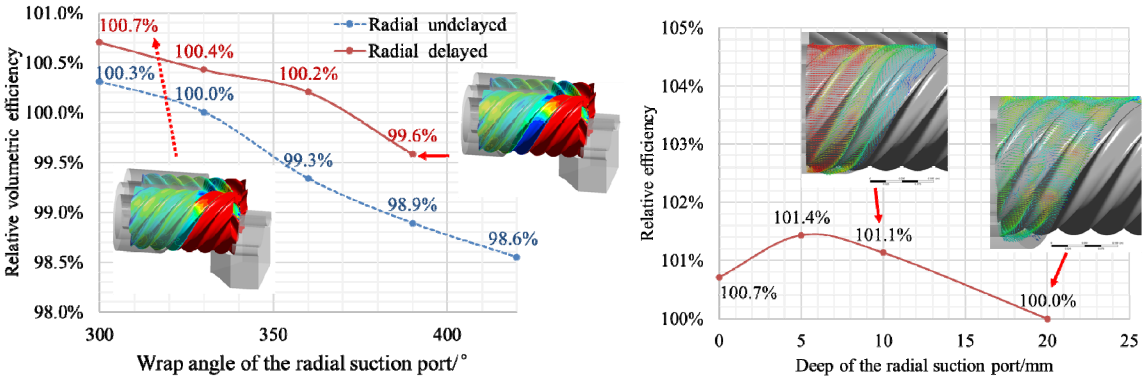

(a) Shape of the suction port (b) Depth of the suction port

Figure 10: Design parameter of the suction port

The most important design parameter of the discharge port is the built-in volume ratio Vi, which is also investiaged, as shown in **Figure 11**. By comparing fluid density in the inlet and out port with 80% isentropic efficiency, the ideal Vi is about 2.47. The efficiency can be improved by slightly enlarging the discharge port with lower resistance, but also can decrease due to insufficient compression. Therefore, an enlarged discharge port with 2.35 Vi is recommended.

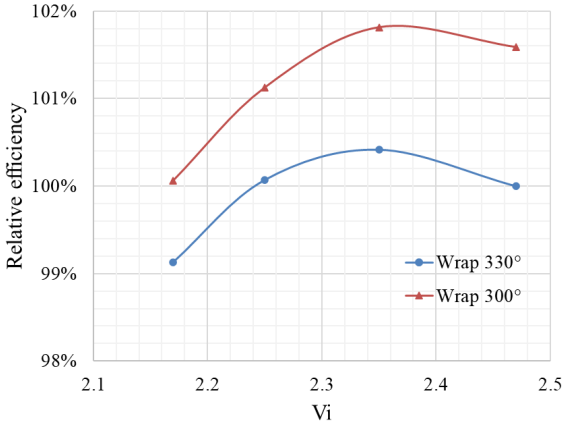

Figure 11: Relative efficiency with Vi

4. CONCLUSIONS

Based on CFD simulations, the design parameters of a screw compressor for chillers at high speed were investigated. Althogh further experimental vaildaiton is needed, several conclusions are summarized as follows:

- The CFD result is more sensitive to axial divisions than radial divisions in the mesh, and the axial division is recommended to exceed 100 for medium-scale compressors. The NRBC condition is vital to speed up simulations at high speed and capture more accurate pulsation. A damping method that introduces a time-dependent source term is helpful for simulations to speed up with more stability. The injected oil in the simulation can hardly influence the mass flow rate and can be neglected.
- When the rotational speed is increased from 3000 rpm to 5000 rpm, the efficiency decays by about 7.5% and the CFD shows the same result. The simulated efficiency decreases by about 3.5% without considering the additional power loss, indicating about 50% influence.

- The 5+6 rotor configuration can be substituted by the 7+8 to reduce the pulsation and noise with a slight performance increase. The L/D ratio can be optimized with the rotor tip velocity not exceeding 0.35Ma. Increasing the wrap angle can help reduce flow resistance and improve performance.
- Suction delay at the axial port can help increase efficiency at high speed, and opening the full axial suction port may help reduce the vibration and noise. Delaying or enlarging the radial port can further increase efficiency, and a deep radial suction port can decrease efficiency through disoriented flow. A smaller than theoretical Vi helps to reduce the resistance to flow, but continuing to reduce Vi results in a loss of efficiency.

REFERENCES

Andres, R., Hesse, J., & Spille, A. (2022). Investigation of radial gap size change under load and the impact on performance for a twin screw compressor using numerical simulation. *IOP Conference Series: Materials Science and Engineering*, *1267*(1), 012007.

Basha, N., Rane, S., & Kovacevic, A. (2018). Multiphase Flow Analysis in an Oil-injected Twin Screw Compressor. *Proceedings of the 3rd World Congress on Momentum, Heat and Mass Transfer*, *April*.

Cambio, M., Branch, S., Scala, A., & Harrison, J. A CFD Investigation Of The Suction Process In A Screw Compressor. International Compressor Engineering Conference. 2021. Paper 2654.

Kameya, H., Ishikawa, M., & Saito, T. (2011). Improvement of volumetric efficiency for screw compressors using inertial charging. In *Institution of Mechanical Engineers - 7th International Conference on Compressors and Their Systems 2011*. Woodhead Publishing Limited.

Kovacevic, A., Rane, S., & Stosic, N. (2014). Screw compressor with variable geometry rotors - analysis of designs by CFD. *Fluid Machinery Congress 6-7 October 2014*, *January*, 91–101.

Pascu, M., Heiyanthuduwage, M., Mounoury, S., Cook, G., & Kovacevic, A. (2013). A study on the influence of the suction arrangement on the performance of twin screw compressors. *ASME International Mechanical Engineering Congress and Exposition, Proceedings (IMECE)*, *7 A*.

Rane, S., Kovacevic, A., Stosic, N., & Kethidi, M. (2013). Grid deformation strategies for CFD analysis of screw compressors. *International Journal of Refrigeration*, *36*(7), 1883–1893.

Rane, S., Kovacevic, A., Stosic, N., & Kethidi, M. (2014). Deforming grid generation and CFD analysis of variable geometry screw compressors. *Computers and Fluids*. https://doi.org/10.1016/j.compfluid.2014.04.024

Rane, S., Kovačević, A., Stošić, N., & Smith, I. (2021). Analysis of real gas equation of state for CFD modelling of twin screw expanders with R245fa, R290, R1336mzz(Z) and R1233zd(E). *International Journal of Refrigeration*, *121*, 313–326.

Sun, S., Wu, X., Li, D., Wang, C., & Xing, Z. (2022). Study on suction pressure loss near suction end and stagnant pressure rise in p- θ diagram of Twin-screw refrigeration compressor for chiller. *Thermal Science and Engineering Progress*, *34*(July), 101410.

Sun, S., Xing, Z., Li, Y., Su, P. C., & Chen, W. (2021). Experimental investigation on twin screw refrigeration compressor with different capacity control methods. *International Journal of Refrigeration*, *130*, 370–381.

Utri, M., & Brümmer, A. (2016). Improvement of the Efficiency of Twin-Screw Refrigeration Compressors by means of Dual Lead Rotors * Corresponding Author. *International Compressor Engineering, Refrigeration and Air Conditioning, and High Performance Buildings Conferences*, *2014*, 1–10.

Utri, M., & Brümmer, A. (2017). Energy potential of dual lead rotors for twin screw compressors. *IOP Conference Series: Materials Science and Engineering*, *232*(1). https://doi.org/10.1088/1757-899X/232/1/012018

Wang, B., Wu, X., Wang, C., & Zhang, Z. (2023). Study on Non-uniform Internal Pressure Distribution of Twin-screw Refrigeration Compressor. *International Journal of Refrigeration*.

Wang, B., Wu, X., Wang, C., Zhang, Z., Li, Y., & Xing, Z. (2024). Performance improvement of twin screw refrigeration compressors for chillers by modifying the suction arrangement. *International Journal of Refrigeration*, *158*, 100–110.

ACKNOWLEDGEMENT

We gratefully thank Gree Electric Appliances, State Key Laboratory of Air-Conditioning Equipment and System Energy Conservation for providing the experimental equipment. This work was supported by the National Natural Science Foundation of China [grant number 52206021, 51976148]; and the High-Performance Calculation Platform in Xi'an Jiaotong University is highly appreciated for the support in the CFD calculation.